JOURNAL OF COLLOID AND INTERFACE SCIENCE 157, 1-13 (1993)

Growth Mechanisms of Iron Oxide Particles of Differing Morphologies from the Forced Hydrolysis of Ferric Chloride Solutions[1]

JOSEPH K. BAILEY,*,[2] C. JEFFREY BRINKER,* AND MARTHA L. MECARTNEY †

Ceramic Synthesis and Inorganic Chemistry, Department 1846, Sandia National Laboratories,[3] Albuquerque, New Mexico 87185-5800; and † Department of Mechanical Engineering, Materials Division, University of California, Irvine, Irvine, California 92717

Received June 1, 1992; accepted October 2, 1992

Since the original work of Matijevic and Scheiner (*J. Colloid Interface Sci.* 63, 509 (1978)) there has been much interest in the unique morphologies of colloidal particles that can be precipitated from ferric salt solutions. To determine the growth mechanisms responsible for the different morphologies, we used time resolved transmission electron microscopy to follow the growth of iron oxide particles produced by the forced hydrolysis of ferric chloride solutions. The growth of three different hematite particle morphologies were investigated: cubes, spheres, and so-called "double ellipsoids." The morphology of the particles depends on the concentration of $FeCl_3$, the pH, and the temperature of aging. All solutions were seen to first produce rod-like particles of akaganéite (β-FeOOH) which would then transform to hematite (α-Fe_2O_3), leading under different conditions to spheres, cubes, or double ellipsoids. For all solutions, the initially produced akaganéite rods form by homogeneous nucleation and subsequent growth. The hematite particles are produced by dissolution of the akaganéite rods and reprecipitation as hematite. For the double-ellipsoid-producing solution, the akaganéite rods remain unaggregated in solution. Hematite heterogeneously nucleates on these rods. In addition to growing outward, the hematite particle uses the rod as a template, and a collar forms, which grows along the rod, producing the double-ellipsoid shape. For a sphere-producing solution, the β-FeOOH rods also remain unaggregated in solution but the akaganéite rods which are formed are shorter than those formed for the double-ellipsoids, and the rods dissolve before the growing hematite particles can use the rods as templates. For the cube-producing solution, the initially produced akaganéite rods aggregate into rafts. These rafts, formed from rods of similar length, have a cubic shape that they impart to the hematite which nucleates on the akaganéite raft. The findings indicate that the concentrations of starting compounds not only influence the kinetics of the reaction, but also influence the colloidal behavior. It is this influence on colloidal behavior that allows a similar chemistry, i.e., the chemistry of dissolution and redeposition of aqueous iron species, to produce different morphologies of precipitated particles.

INTRODUCTION

Colloidal solutions of monodisperse particles are important for producing model systems for understanding aggregation, flocculation, and precipitation, and also for developing experimental techniques such as light scattering and rheometry of colloidal solutions. Although spherical particles are the most easily modeled, other particle morphologies such as rods, ellipsoids, and cubes are important for developing theories for complex systems. Therefore, it is not surprising that the work of Matijevic and Scheiner (1), which demonstrated that iron oxide and oxy–hydroxide particles could be formed in many different morphologies using precise control of the chemistry, led to a significant amount of interest in using these particles as model colloids. A selected list of papers which describe research using these particles includes studies in optical property characterization (2, 3), rheology and magneto-rheology (4), adsorption (5), aggregation behavior (6), ion exchange (7), and water chemistry (8).

Beyond production of model colloidal suspensions, solution methods for precipitation of oxide powders are increasing in importance for preparation of ceramic powders for advanced ceramic applications. To obtain an ability to tailor the material processing to the application, it is necessary to understand the growth mechanisms which lead to uniform, monodisperse, unagglomerated powders. If we can control the growth of the powders to produce uniform monodisperse powders and can precipitate the powders in well-packed compacts, we can make ceramics with higher green densities, fewer defects, and better properties. For these reasons, it is important to investigate the growth mechanisms which lead to particles of varying shape to understand the influence of the processing conditions on the final particle morphology.

In particular, for iron oxide powder precipitation, particles of many different morphologies have been produced, and

[1] Work performed at Sandia National Laboratories supported by the U.S. Department of Energy (DOE) under Contract DE-AC04-76-DP00789.

[2] To whom correspondence should be addressed at current address: 3M Company, 3M Center, Building 236-3C-02, St. Paul, MN 55144-1000.

[3] A U.S. DOE facility.

0021-9797/93 $5.00

thus control over the resultant colloid morphology has been demonstrated. Matijevic and Scheiner (1) demonstrated that small changes in reaction environment can produce large changes in particle morphology. Changes in pH, counter-ion, temperature, and solvent have all been shown to be important variables which must be controlled during processing in order to produce uniform monodisperse colloids. The chemistry of the precipitation of iron oxides from ferric salt solutions has been well studied. Matijevic and Scheiner's experiments laid the groundwork for this topic when they conducted a series of experiments which mapped out the particle morphology space experimentally, producing tables that relate ferric salt concentration, acid concentration, and time to particle morphology. More recently Matijevic and Blesa (9) have reviewed the literature regarding the likely chemical mechanisms which lead to the precipitation.

Particles of several different morphologies can be precipitated from ferric chloride solutions. The major particle shapes are rods, spheres, cubes, and curiously shaped double ellipsoids. The phase of the rod-shaped particles is akaganéite, β-FeOOH; for the other particle shapes it is hematite, α-Fe_2O_3. For the precipitation of hematite from ferric chloride species, it has been shown that particles with the akaganéite phase form first and then transform into hematite through dissolution and reprecipitation (9). The chemistry for the process is usually discussed with regard to the species in solution without regard for the morphology of the particles, and therefore it is assumed that the same chemical reactions produce the various shapes of hematite particles. A short review of this chemistry follows.

Ferric chloride, when dissolved in water, undergoes displacement of the chloride ligands, forming a hydrated ferric ion (10). Above pH 0.5–2 (depending on ionic strength), the hydrated ferric ion undergoes hydrolysis to form a species with tightly bound hydroxide ions in addition to loosely bound water molecule ligands. The hydroxide ligands on separate ferric ions can then react by olation or oxolation to form complexes with iron atoms linked by bridging oxygen atoms. For the pH ranges studied in this work (0.8 to 1.8) the predominant aqueous species in solution are expected to be monomers and dimers with zero to two hydroxide ligands per iron atom (10). If the concentration of these molecules is higher than the saturation concentration, then, in addition to the aqueous species, solid hydrous iron oxides will also form. The solid that initially forms from ferric chloride solutions is akaganéite, β-FeOOH. It has been strongly argued that the reason that akaganéite forms from ferric chloride solutions is due to a specific interaction of the chloride ions with the surface of the hydrous iron oxide (11–13).

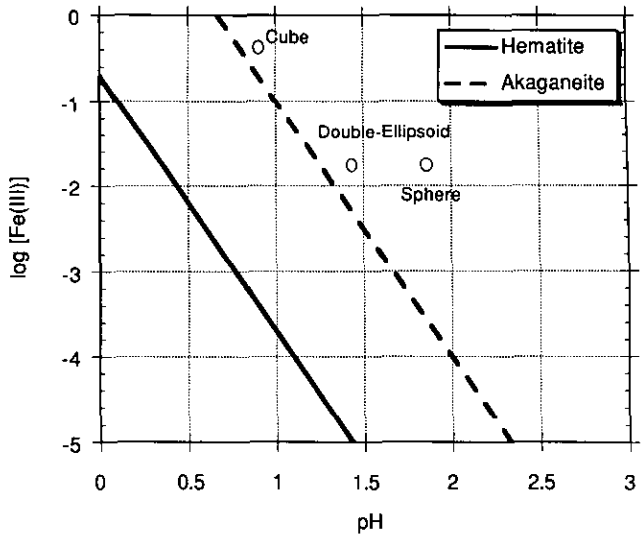

FIG. 1. Approximate solubility diagram for Fe(III) ion. Saturation lines are denoted for akaganéite (β-FeOOH) and hematite (α-Fe_2O_3). After Flynn (14) for ionic strength 0. Starting compositions of solutions used in this work are indicated.

The transformation of akaganéite to hematite takes place if the temperature of aging, the solution pH, and the concentration of iron are high enough. It is known that this transformation must be a dissolution and reprecipitation reaction since the transformation from akaganéite to hematite does not take place when dry akaganéite particles (thus avoiding dissolution) are aged at the same temperatures, 100–150°C, which would result in transformation if the particles were in an aqueous liquid medium (9, 14).

Figure 1, adapted from Flynn (14), shows a solubility diagram for ferric ion, akaganéite, and hematite. Also shown in Fig. 1 are the starting compositions of the solutions analyzed in this study. Akaganéite forms faster since it has a lower energy for nucleation (9). Hematite, however, is a more stable crystal structure with a solubility lower than that of akaganéite. Therefore as the akaganéite grows it depletes the ferric ion concentration in solution until the concentration approaches the saturation level of akaganéite. When hematite nucleates and grows, the concentration can fall below the saturation concentration for akaganéite, thus the akaganéite then dissolves.

DeBlanco *et al.* (15) have suggested that the growth mechanism for this process is the simultaneous nucleation of hematite and akaganéite, with akaganéite nucleating at a

FIG. 2. Ferric hydrous oxide particles produced by aging sphere-forming solution (0.018 *M* $FeCl_3$, 0.01 *M* HCl) at 100°C. (a) Dried-sample TEM micrograph from sample aged for 12 h. (b) Sample prepared by cryo-TEM technique after aging for 12 h. (c) β-FeOOH and α-Fe_2O_3 particle formed after 24 h. H denotes α-Fe_2O_3 particle, A denotes β-FeOOH particle. (d) α-Fe_2O_3 particles produced after 1 week, inset shows diffraction pattern from a single α-Fe_2O_3 particle; zone axis is [4 0 5].

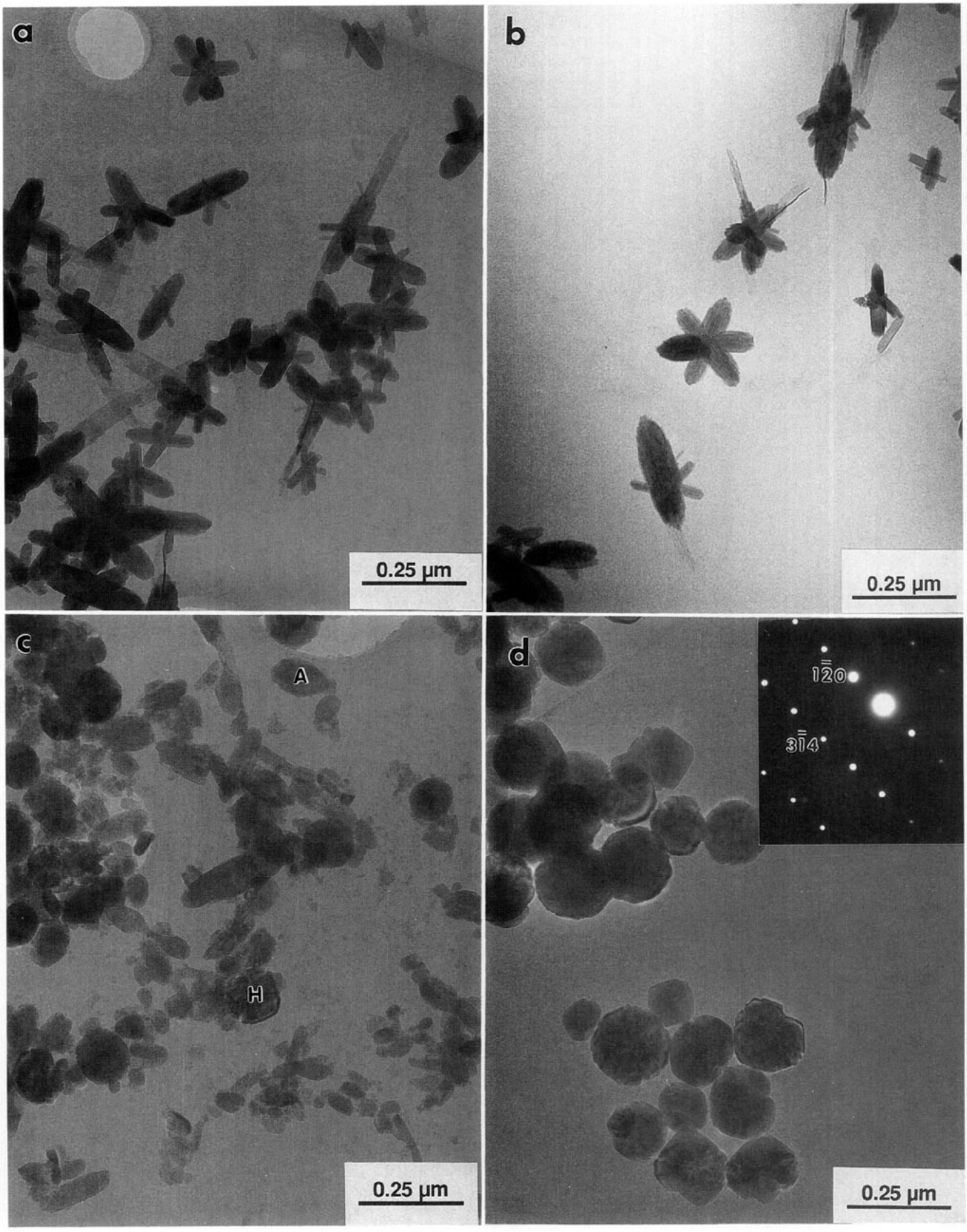
a
0.25 μm
b
0.25 μm
c
A
H
0.25 μm
d
$\bar{1}\bar{2}0$
$3\bar{1}\bar{4}$
0.25 μm

much higher rate than hematite. After particles grow until the concentration of ferric ion is below the saturation concentration for akaganéite, the hematite grows at the expense of the akaganéite. However, the mechanism of simultaneous nucleation has not been confirmed for a wide range of conditions. The mechanism that controls the morphology of the hematite particles is also still unclear, since it is proposed that a similar chemistry is operative for all the solutions regardless of morphology (9).

In our study, time resolved transmission electron microscopy (TEM) is used to follow the precipitation of four different particle morphologies: spheres, double ellipsoids, rods, and cubes. Dried sample TEM has previously been performed on iron oxides, primarily for phase identification of the final products. Time resolved studies were used by Quirk and co-workers (16–18) to identify growth mechanisms during the neutralization of basic iron solutions of ferric chloride. For forced hydrolysis of ferric chloride solutions, DeBlanco *et al.* (15) have used time resolved dried sample TEM to examine the growth mechanism of cubic particles. This study compares and contrasts the growth mechanisms of different particle morphologies using dried sample TEM and fast-frozen cryogenic TEM (cryo-TEM). Cryo-TEM is a technique in which fast frozen liquid films are directly imaged, allowing one to directly observe the sol structures in the wet state. It has previously been used to image the growth of silicate gels and colloids and vanadium oxide particle formation (19–21). Through the study of the precipitation of silica colloids from solution using both dried sample and cryo-TEM techniques, it has been demonstrated that dried sample preparation techniques can lead to artifacts that can misrepresent the actual sol, gel, or precipitate structures (20).

MATERIALS AND METHODS

Materials

All chemicals were reagent grade and were used without further purification. Water was distilled and deionized through a commercial Millipore unit. Concentrated stock solutions of reagent grade ferric chloride (Mallinckrodt) were made at approximately 3.0 *M*. These stock solutions were then used to prepare the ferric chloride solutions for the precipitation reactions.

Preparation of Sols

Three different solutions were used in this study: the "cube solution" contained 0.45 *M* $FeCl_3$ and 0.01 *M* HCl. The "sphere solution" contained 0.018 *M* $FeCl_3$ and 0.01 *M* HCl. The "double-ellipsoid" solution contained 0.018 *M* $FeCl_3$ and 0.05 *M* HCl. The concentrations for these solutions were all taken from the work of Matijevic and Scheiner (1). A separate rod solution was not prepared, since all of the above solutions initially formed rods and thus gave sufficient insight into the rod formation mechanism. After preparation of 100 ml of solution, approximately 10 ml of solution was pipetted to several screw-capped culture tubes which were then placed in a preheated oven and kept at constant temperature for the desired aging time. For these samples, some batches were heated in a gravity oven, while other samples were heated in a forced air convection oven. No significant difference was seen between the sphere and cube samples heated in the different ovens. Slight differences were seen in the double-ellipsoid solutions and these will be discussed later. After aging, the samples were cooled to room temperature. All solutions were kept in their mother liquors until electron microscopy samples were prepared. Vigorous shaking was used to redisperse settled sols.

Electron Microscopy

Transmission electron microscopy samples were prepared by two different methods: a dried sample preparation technique and cryo-TEM preparation. Both sample preparation techniques used the colloids in their mother liquors; no washing or centrifugation was performed.

In the dried sample preparation technique, a drop of sol from the reaction vessel was placed directly onto a holey carbon support grid which was laying on filter paper. Most of the solution flowed through the holes in the grid, minimizing aggregation of the particles which were trapped on the surface of the grid. Control of the drop size is critical for minimizing aggregation of the particles during deposition. Drop sizes were between 3 and 9 μl and were dispensed with a Eppendorf micropipette. The samples were then air dried. Three transmission electron microscopes were used for the dried sample work, a JEOL 100CX, a JEOL 2000FX, and a Philips CM-30.

Although the dried sample preparation technique is relatively simple to perform, it can produce drying artifacts which can lead to erroneous interpretation of TEM data (20). Therefore a cryo-TEM sample preparation technique, which does not produce drying artifacts, was used to image the structures present in the liquid state (22, 23). The cryo-TEM technique involves fast freezing thin liquid films of solution to instantaneously vitrify the solvent and to trap the particles present without rearrangement. A controlled environment

FIG. 3. Ferric hydrous oxide particles produced by aging double-ellipsoid solution (0.018 *M* FeCl3, 0.05 *M* HCl) at 100°C. The solution designation (A, B, C) refers to separate batches of nominally the same solution, see text for details. In the micrographs, H denotes hematite phase, A denotes akaganéite phase. (a) β-FeOOH particles formed after aging sample for 1 h (solution A). (b) High-resolution TEM micrograph showing crystalline orientation of β-FeOOH rods (solution C). Inset shows diffraction pattern of rod, zone axis is [010]. (c) High-resolution TEM micrograph of β-FeOOH rods contained in star. Arrow denotes boundary area where rods are attached.

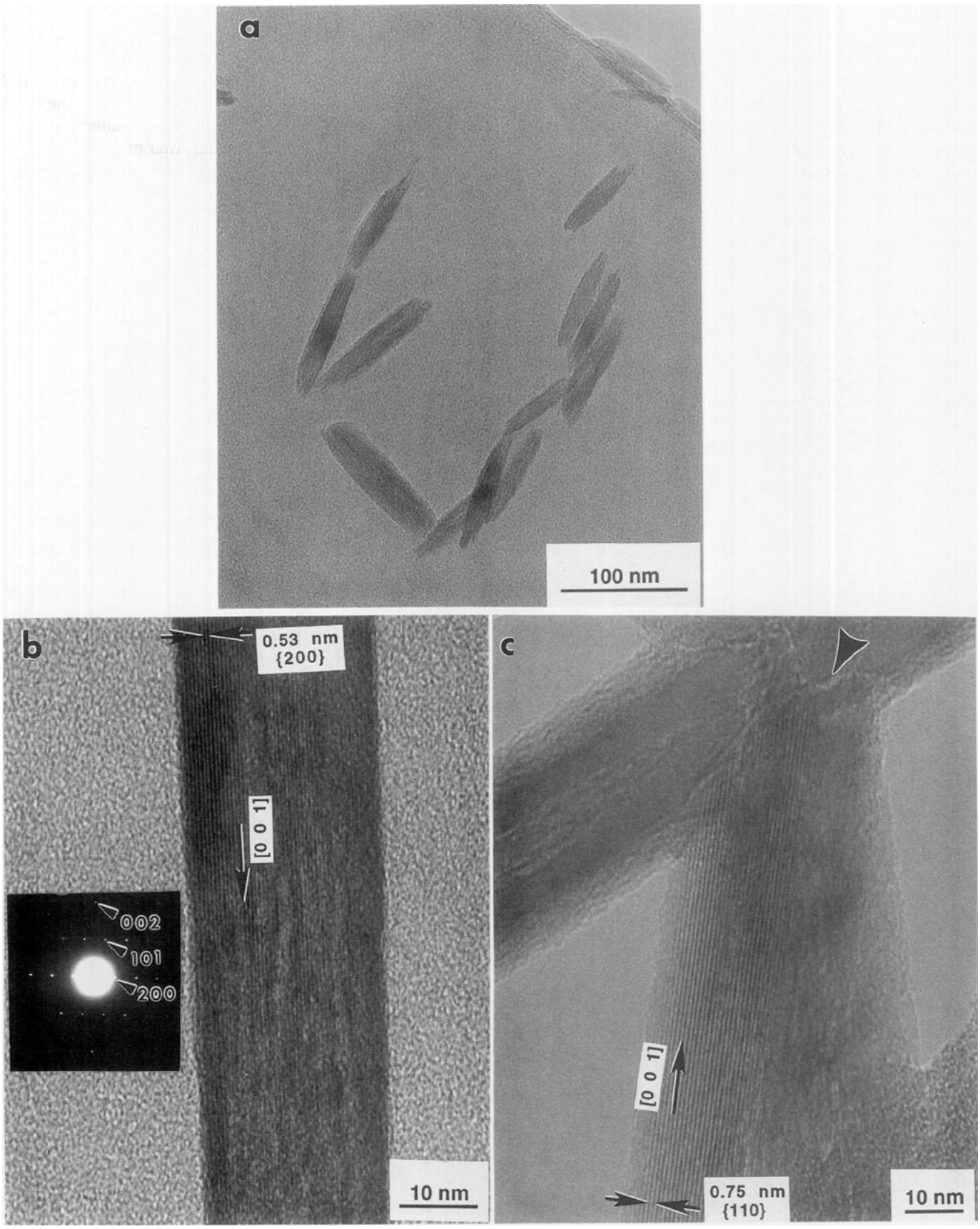
a
100 nm
b
0.53 nm
{200}
[0 0 1]
002
101
200
10 nm
c
[0 0 1]
0.75 nm
{110}
10 nm

vitrification system was used for the preparation of samples. Holey carbon grids were placed in the environmentally controlled chamber, which was saturated with water vapor. A drop of the reacting solution was placed on the grid at the desired point in the reaction, and the sample was blotted to form thin liquid films spanning the grid holes. The sample was then plunged into liquid ethane, which froze the liquid at cooling rates greater than 10,000 K/s. This cooling rate was fast enough to solidify the solvent but maintain its amorphous structure, with very little volume change. This rapid cooling trapped the particles in the amorphous vitrified matrix without rearrangement, thus preserving the liquid state structure. The sample was then transferred to a cold stage using a cold stage transfer module and imaged in the electron microscope directly. This technique is discussed more fully elsewhere (22, 23). For this work, a Gatan cold stage and cold stage transfer module were used with a Philips CM-30 transmission electron microscope.

RESULTS

Spheres

The sequence of structural development for the spheres is shown in Figs. 2a–2d. Figure 2a shows rods that have formed from ferric chloride solutions aged for 12 h at 100°C. The rods were identified as β-FeOOH from the electron diffraction patterns. For all the rods studied, the $\langle 001 \rangle$ direction is the long direction of the rods. The rods seen in Figs. 2a and 2b are arranged predominantly in star-shaped clusters of rods. Note that the akaganéite crystal structure is tetragonal, with an a/c ratio of unit cell dimensions of 3.477. To determine if the star-shaped structures were sample preparation artifacts caused by drying the sample, cryo-TEM samples were prepared from this solution at 12 h of reaction time. The cryo-TEM micrograph (Fig. 2b) shows that the star-shaped particles are also seen in the fast-frozen thin liquid film, thus this morphology must form in solution.

The structures present in the solution after 24 h of aging at 100°C are shown in Fig. 2c. In this micrograph, there are both β-FeOOH particles and α-Fe_2O_3 particles present. The spherical hematite particles, labeled H in Fig. 2c, are found separately from the pieces of β-FeOOH rods, labeled A. Figure 2d shows the final morphology of the particles, approximately 0.25 μm in diameter, after 1 week of aging at 100°C. Although the particles are not perfectly spherical, they lack a definitive shape and are approximately uniaxial. Figure 2d also shows that the particles have some faceting. Electron diffraction patterns indicated that all individual particles were single crystal particles of hematite, as shown by the representative diffraction pattern inset on Fig. 2d for a single sphere.

Double Ellipsoids

As with each morphology, several double-ellipsoid solutions were prepared for this investigation. They were nominally the same concentration and were aged at nominally the same temperature; however, there was greater variability among the separate batches of double-ellipsoid-forming solutions than for either the sphere- or the cube-forming solutions. Since different batches were prepared in different locations and aged in different ovens, slight variations in concentrations and aging may have occurred. All solutions produced particles with the double-ellipsoidal shape; however, there were differences in the particles in terms of the length-to-width ratio of the ellipsoids. In order to differentiate the samples which were taken from the different solutions, the solutions are labeled A, B, and C. Solution A was aged in a gravity oven, with the temperature monitored by a mercury thermometer located near the samples. Solutions B and C were aged in a forced convection oven, with the temperature-control thermocouple located near the samples.

The sequence of structural development for the double-ellipsoid particles is seen in Figs. 3–6. Figure 3 shows the early reaction products. The reaction products at 1 h of reaction, taken from solution A, are shown in Fig. 3a. Similar to the sphere-forming solutions, rods of akaganéite have formed. At 4 h, some star-shaped particles were observed, similar to those found in the sphere-forming solution, c.f. Fig. 2a and 2b. However, for the double-ellipsoid-forming solutions, the rods comprising the stars were longer, approximately 800 nm long at 4 h, compared to 300 nm for the sphere solutions. Figure 3b shows a high-resolution TEM micrograph of a rod with diffraction pattern inset. The zone axis of the diffraction pattern is [010]. Figure 3b shows that the rods are single crystal, with the long axis of the rod parallel to the c-axis. Figure 3c shows a high-resolution TEM image of a rod contained in a star, showing the orientation of the crystal structure. Again, the $\langle 001 \rangle$ direction is always the long direction of the rods. Also seen in Fig. 3c are grain boundaries where the individual rods which comprise the star join together, indicating that not all rods are continuous across the star.

Hematite particles are observed later in the reaction. The hematite particles were attached to rods of akaganéite, as shown in Fig. 4. Figures 4a and 4b were taken from solution C after 6 h of reaction. After 8 h, rods are again seen with

FIG. 4. Ferric hydrous oxide particles produced by aging same solution as in Fig. 3 at later times of reaction. (a) α-Fe_2O_3 particle growing on β-FeOOH rod after aging for 6 h (solution C). (b) α-Fe_2O_3 particle growing on β-FeOOH rod after aging for 6 h (solution C). (c) α-Fe_2O_3 particle growing on β-FeOOH rod after aging 8 h (solution B). (d) α-Fe_2O_3 double ellipsoid formed after 8 h of aging (solution B). Small rod denoted by arrow indicates β-FeOOH rod in center of particle.

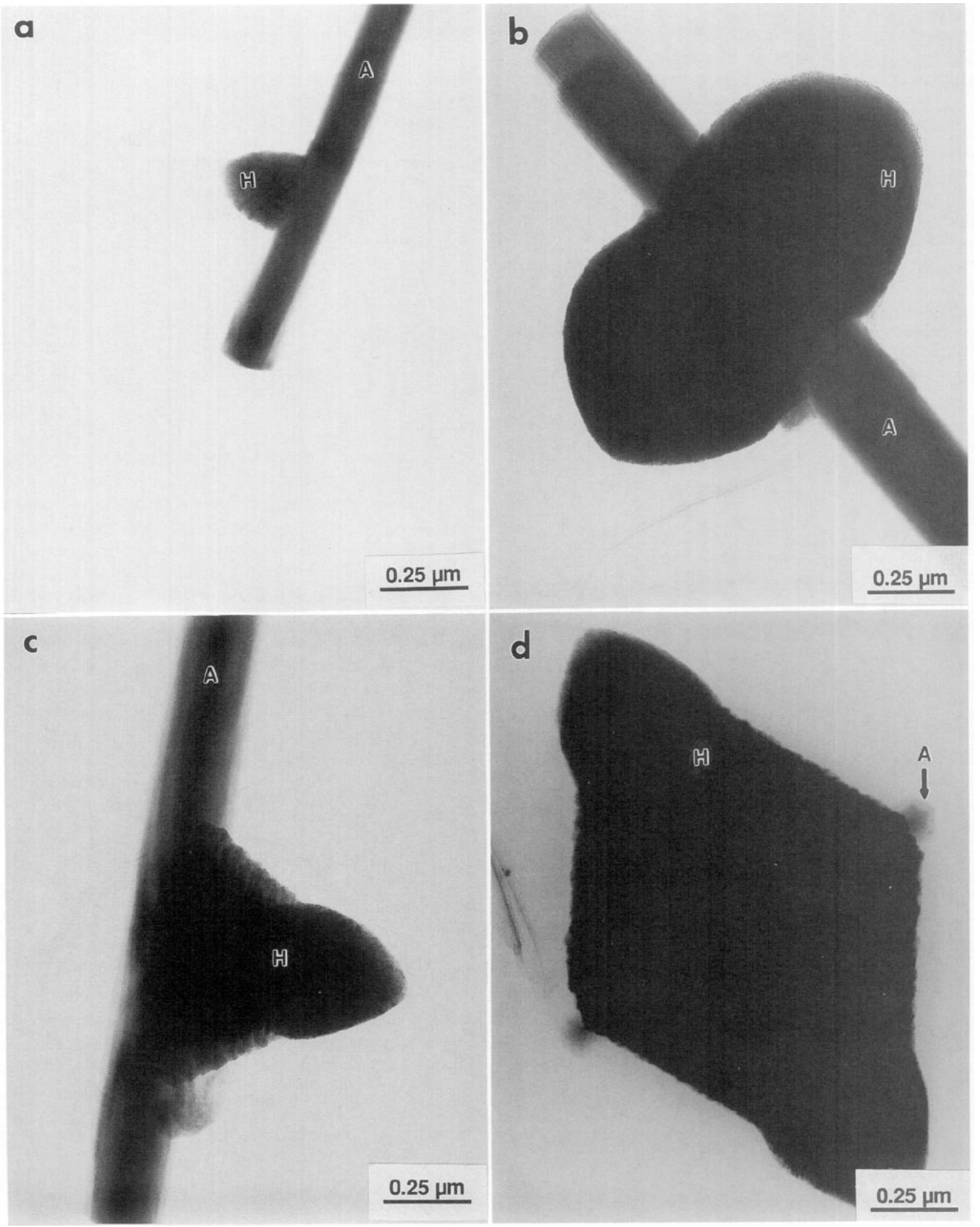
a
A
H
0.25 μm
b
H
A
0.25 μm
c
A
H
0.25 μm
d
H
A
0.25 μm

particles attached (Figs. 4c and 4d—solution B); however, comparison with Figs. 4a and 4b shows that the particles have grown in size and are surrounded by a collar where they attach to the akaganéite rods.

Although Figs. 4a and 4c show particles growing on only one side of the akaganéite rods, these represent the minority particles, as only approximately 10% of the particles observed were single-sided particles. Most of the particles were double ellipsoids, as seen in Figs. 4b and 4d. These double-ellipsoid particles incorporate a rod of akaganéite, which bisects the double ellipsoid. Figure 4d shows that the rod of akaganéite is located exactly in the middle of the particles and that the collars formed in this solution are quite large.

It was also noted that each individual double-ellipsoidal particle examined by electron diffraction had a slight rotation between the two halves of the double ellipsoid. Figure 5 is from a sample aged 24 h at 100°C (solution A) and shows that these elongated ellipsoidal particles are bicrystals, with the one-half crystallographically rotated with respect to the other half. In Fig. 5, the particle is shown along with the diffraction pattern for the top half of the particle, denoted by the letter X, and the diffraction pattern for the bottom half of the particle, denoted by the letter Y. Also shown (the middle diffraction pattern) is the diffraction pattern taken using a larger selected-area aperture which gives the diffraction for the entire particle. This diffraction pattern displays two sets of spots, one for each half of the particle, rotated 4° about the [3 4 1] zone axis. Lastly, the double-ellipsoidal particles (solution C), approximately 1 μm in length at 1 week of aging time, are shown in Fig. 6.

Cubes

The sequence of structural development for the cubes is shown in Fig. 7. A cryo-TEM sample taken after only 13 min of heating indicated that rods of akaganéite had formed in these solutions (Fig. 7a). Unlike the sphere and double-ellipsoid-forming solutions, however, there were no star-shaped particles in these solutions; instead, the rods had aggregated into rafts of particles, with each raft containing only similar size rods. Since this was a cryo-TEM sample, these rafts are not drying artifacts, and the particles are organized into rafts in the liquid state. Both dried sample and cryo-TEM micrographs taken after more aging showed that the rods of akaganéite were still present and were still aggregated into rafts; however, the particles had grown, the aspect ratio of the rods had increased, and the size distribution of rod sizes had narrowed. Figure 7b was taken from a cryo-TEM sample after 1 h of aging and shows that the rods of akaganéite have grown, but are still aggregated into rafts. Figure 7c shows rafts of rods from a dried TEM sample after 3 h of aging and the diffraction pattern from a single raft. The akaganéite diffraction spots in this diffraction pattern show that all rods have the $\langle 001 \rangle$ direction being the long direction of the rods and the rods are highly aligned, resulting in the dark bands running perpendicular to the direction of the rods. In addition to the akaganéite diffraction spots in this pattern, there are also spots which cannot be attributed to akaganéite, but correspond to diffraction from hematite. These spots indicate that somewhere within the raft, hematite has nucleated.

At later times, cubic particles are seen, but they are too thick to be transparent in the electron microscope, even at 300-kV accelerating voltage. When the thick cuboidal particles are seen, the solution has begun to turn from a yellowish to a black sol, whereas the solutions which formed spheres and double ellipsoids became red as the hematite particles formed. X-ray diffraction confirmed that the yellowish particles were akaganéite and that the black particles were hematite. Figure 7d shows the morphology of the cubic particles, approximately 1.5 μm in size, which have formed after 24 h at 150°C.

DISCUSSION

From this electron microscopy investigation, two fundamental similarities were observed between these three different systems. First, the solutions all initially produce akaganéite rods. The rods differ in length, aspect ratio, and mode of aggregation, but all systems form rods. Second, the rods evolve into hematite particles. Regardless of the morphology, all particles were hematite at the end of the reaction. The object of this section is to explore why the different morphologies form and elucidate the role of aggregation in determining the final morphology.

Formation of Akaganéite Rod- and Star-Shaped Particles

Rods of akaganéite apparently form by homogeneous nucleation and subsequent growth by addition of soluble species at the ends of the rods. It is not a single burst of nucleation because a broad range of rod sizes are seen early in the reaction (see, for example, Fig. 7a). High-resolution TEM micrographs, e.g., Fig. 3b, indicate that the individual rods are single crystal akaganéite with no hematite phases present. This result is consistent with the results of MacKay (12). The rods grow preferentially lengthwise. Figure 7a, a cryo-TEM micrograph, shows the rods as they appear in the liquid. From this and similar micrographs, we see that the growth occurs at finger-like projections at the ends of the rods. Figure 7b, a cryo-TEM micrograph taken at a later time, shows that the ends of the rods become smoother with time, likely due to the decrease in solubility due to the large negative curvature that occurs between the finger-like growths at the ends of the rods.

Our hypothesis for the formation of the star-shaped particles is that one or more heterogeneous nucleation sites occurs on the first rod that forms, creating the branches of the

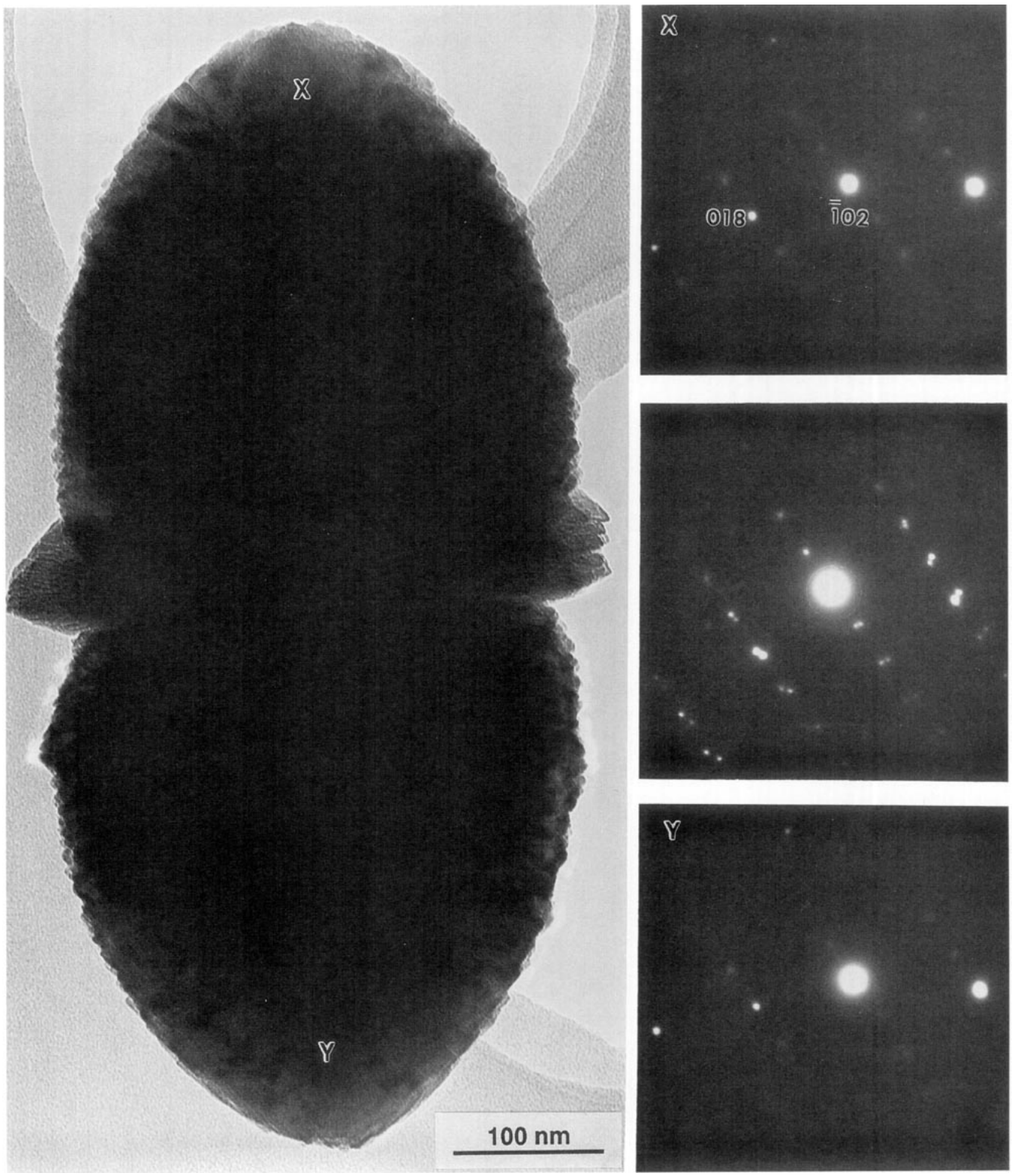

FIG. 5. α-Fe_2O_3 double-ellipsoid produced by aging same solution as in Fig. 3 for 24 h (Solution A). Diffraction pattern denoted X is from half of particle marked X, diffraction pattern denoted Y is from half of particle marked Y, middle diffraction pattern is from entire particle. Zone axis for diffraction patterns is [3 4 1].

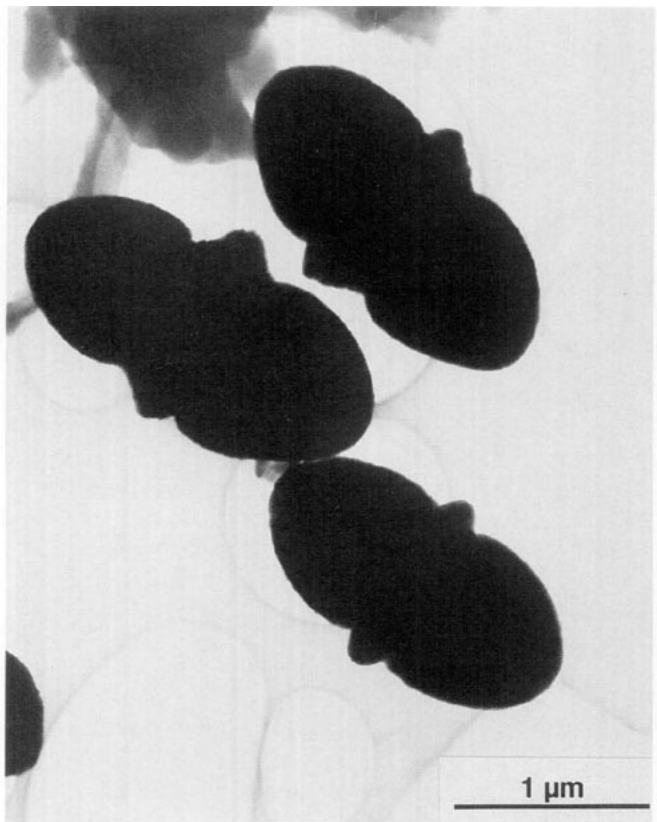

FIG. 6. α-Fe_2O_3 double-ellipsoid produced by aging same solution as in Fig. 3 for 1 week at 100°C.

star. MacKay (12) showed that the (332) plane is a twin plane in the β-FeOOH crystal structure, with components of the twinned crystals laying only along the (110) planes. Such a twin configuration could produce two rods, elongated along the c-axis, intersecting at 63° (12). Thus, it would not be crystallographically unfavorable for the initially nucleated rod to grow branches and form a star since growth along the $\langle 001 \rangle$ direction can occur if it intersects the initial rod at 63°. Furthermore, Paterson and Rahman (11) have shown that chloride ions are incorporated into the surface of β-FeOOH rods; thus, the surface of the rods is not pure β-FeOOH. In the present study, the solution which gave rise to the most stars was the sphere-forming solution, the double-ellipsoid-forming solution produced fewer stars, and the cube-forming solution gave the least stars. This order of star formation is in inverse order of ionic strength, suggesting that chloride ion adsorption on the β-FeOOH hinders star formation. Although there is reason to suspect that heterogeneous nucleation on the initially formed rod gives rise to stars, the above arguments do not suggest why the individual branches of the stars all seem to emerge from the same point.

From the literature (9, 15), there is some evidence for simultaneous nucleation of akaganéite and hematite; hence, another hypothesis could be that hematite nucleates simultaneously with the akaganéite, and that subsequently several akaganéite crystals nucleate heterogeneously on the seed of hematite and grow outward, forming a star. However, there is no evidence in the electron diffraction patterns to support this latter hypothesis. Furthermore, in the case of the double ellipsoids, the hematite particles which form and grow into double ellipsoids do not necessarily form at the centers of the stars.

Formation of Hematite Sphere- and Double-Ellipsoid-Shaped Particles

The first step in the production of sphere-shaped particles is the nucleation and growth of predominantly unaggregated akaganéite rods and stars, as discussed above. These rods then dissolve and reprecipitate as single-crystal, roughly-spherical hematite particles. Figure 2c provides strong evidence for the dissolution of the rods, since much akaganéite debris is seen on the grids. Unfortunately, we are unable to conclude whether the nucleation of the hematite is homogeneous or heterogeneous. However, there are no hematite nuclei in the electron micrographs taken early in the reaction sequence for any of the solutions studied. Thus, it is likely that hematite nucleates heterogenously on the akaganéite. The morphology of the sphere-shaped particles is probably due to the minimum of surface energy which accompanies the spherical shape. Some faceting of the spheres is seen in the micrographs, but predominantly there is no regular polygonal shape to the particles.

The sphere-shaped particles are approximately 200 nm in size and are single crystal, which is unlike the larger (approximately 1 μm polycrystalline spherical particles reported elsewhere in the literature (1, 24). The conditions which produced the smaller, single-crystal particles were a lower $FeCl_3$ concentration and a higher HCl concentration than those for the larger, aggregated, spherical particles. The large HCl concentration produces a higher surface charge which results in greater colloidal stability. Therefore, unlike the previously reported spherical particles, the particles studied in this work can grow in solution as separate single crystals.

For the double ellipsoids, the first step is also homogeneous

FIG. 7. Ferric hydrous oxide particles produced by aging cube solution (0.45 M $FeCl_3$, 0.01 M HCl) at 150°C. (a) Rafts of β-FeOOH particles fast frozen in amorphous ice matrix from cryo-TEM sample prepared after 13 min of aging. (b) Rafts of β-FeOOH particles fast frozen in amorphous ice matrix from cryo-TEM sample prepared after 1 h of aging. (c) Rafts of β-FeOOH rods from dried sample aged 3 h. Diffraction pattern inset from single raft indicates α-Fe_2O_3 is also present in the raft. Letter A refers to akaganéite (400) reflection, d = 0.2634 nm. Letter H refers to hematite (104) reflection, d = 0.270 nm. (d) Cube-shaped α-Fe_2O_3 particle formed after 24 h of aging. Identification of particle phase by X-ray diffraction.

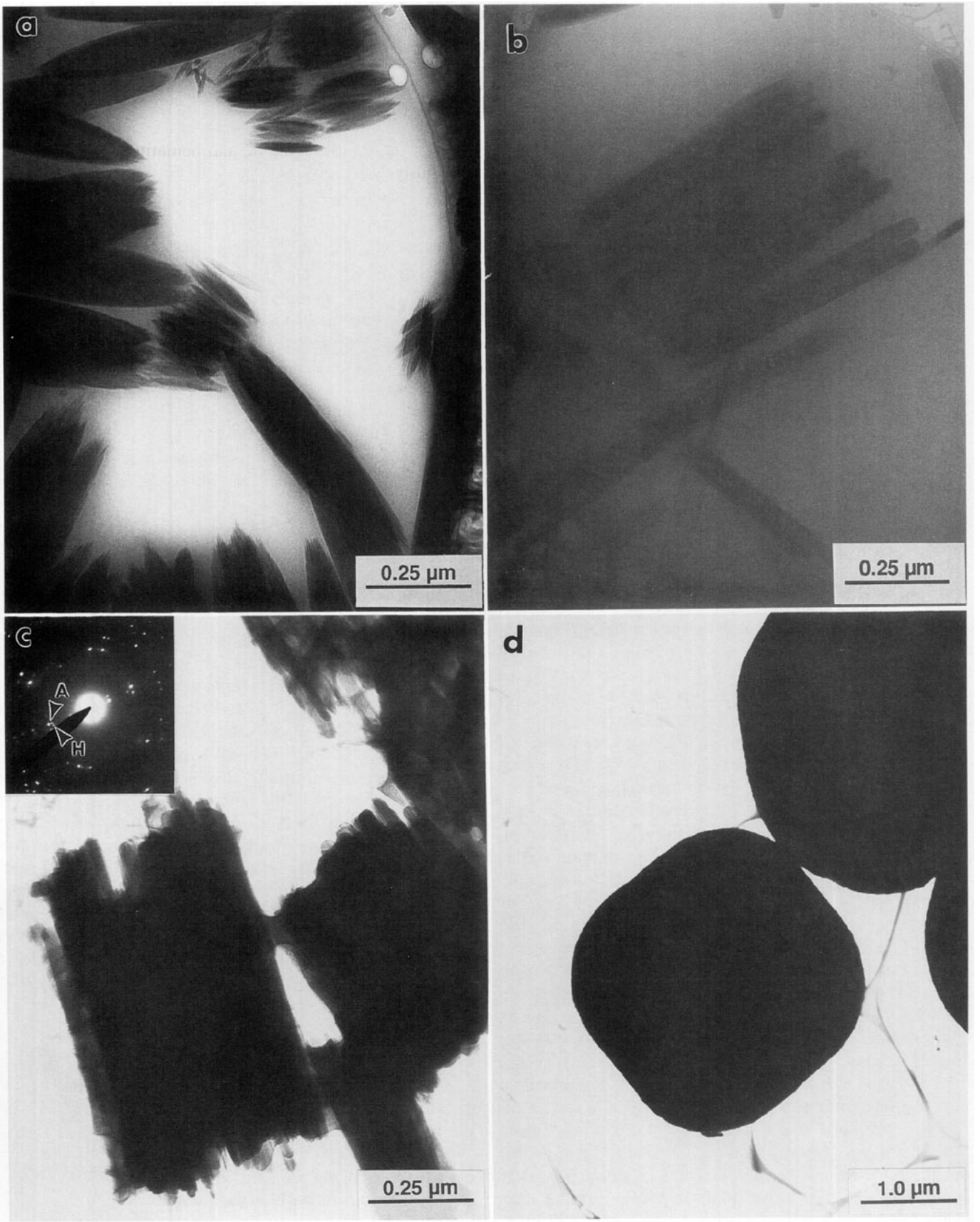
a
0.25 μm
b
0.25 μm
c
A
H
0.25 μm
d
1.0 μm

nucleation of akaganéite rods. For the double-ellipsoid-shaped particles, Figs. 4a and 4b provide evidence of heterogeneous nucleation of the hematite on the akaganéite rods. Once nucleated on the rods, the hematite particles grow in a roughly spherical shape, except for the end attached to the rod. Since the hematite grows faster into the solution than it does along the rod, one can conclude that the surface energy between the akaganéite and the hematite is greater than the surface energy between the hematite and liquid. However, at a time when the contact angle between the hematite particle and the akaganéite rod exceeds approximately 90°, the collar begins growing along the rod. In general, it is known that as the contact angle between particles increases, the curvature becomes more negative and thus the solubility at the contact point decreases (25). This decrease in solubility at the contact point between the hematite and akaganéite leads to a second nucleation of hematite (whose crystallographic orientation is better matched to that of akaganéite), which grows along the rod as a collar of the original hematite particle. In the course of time, the collar builds to a thickness where the particle obtains a double-ellipsoid shape as shown in Fig. 4d. From the electron diffraction patterns of the double ellipsoids, it is seen that they are bicrystals with a slight rotation between the two halves, c.f. Fig. 5. The constraint of the rod on which the hematite crystal is growing must account for the slight rotation in the two halves.

There are similarities between the spheres and the double ellipsoids. For both morphologies, the initially formed akaganéite rods and stars are unaggregated. The hematite then nucleates on the akaganéite rods. The akaganéite rods in the sphere-forming solutions are shorter than the rods in the double-ellipsoid solutions. Thus, spheres form on akaganéite rods which are much smaller than the rods on which the double ellipsoids form. Therefore it is reasonable to speculate that for the sphere-forming solutions the rods dissolve before the hematite particles become large enough that the curvature at the contact point exceeds its critical value for collar nucleation to occur. Hence the spheres never develop collars as do the double ellipsoids. In other words, the rod dissolves before a growing sphere can use the rod as a template for growth. For the double ellipsoids, the rods are longer, and thus survive longer, so the growing hematite particle can grow not only outward, but at some point begin to grow a collar, which uses the akaganéite rod as a template for growth. From Fig. 1, which shows the concentrations of the starting solutions and the saturation concentrations, it is seen that the sphere-forming solutions as initially prepared are more supersaturated than the double-ellipsoid-forming solutions. The sphere-forming solution thus has a higher driving force for nucleation, and one would expect a higher nucleation rate. The higher nucleation rate would lead to more nuclei, and hence the rods in the sphere-forming solution should be shorter than the rods in the double-ellipsoid-forming solution. Therefore, one effect of the starting concentrations is that of controlling supersaturation which determines the nucleation rate and determines whether the akaganéite rods grow to a sufficient length to survive until the growing hematite particles can use them as a template.

Formation of Hematite Cubes

For the cubes, a different growth pattern emerges. Initially rods form, as in the other cases. However, for the cubes, the concentration of all ions is much higher due to a 30-fold increase in the starting $FeCl_3$ concentration. This higher concentration of ions leads to a shorter Debye–Hückel screening length, which leads to a weaker repulsive force from DLVO theory of colloidal interactions (26). Hence, it is not surprising that the rods which form in the cube-forming solution are aggregated. They aggregate into rafts which are comprised of similar-length rods, see Figs. 7a–7c. Whether the rafts exclude rods of different length due to electrostatic or magnetic interactions is not clear, although Heller, who has looked at the aggregation of akaganéite rods, reported that they can be aligned with magnetic fields (27). Weak magnetic moments in the rods could lead to ordered aggregation in the sols.

Due to the thickness of the rafts and the initial cubes, it is impossible to see through the cubes in the electron microscope. Therefore, it is undetermined if the cubes are single or polycrystalline. However, in the raft diffraction patterns, some spots due to hematite are present. This indicates that the hematite nucleates on the rods in the rafts. Due to the shape of the rafts, it then appears that the hematite grows with a cubic shape due to topotactic conversion of the rafts to hematite. This is further supported by the lack of debris in any of the micrographs with the cubic system. Unlike the spheres, in Fig. 2c, where the dissolution of the rods is evident, the cube-forming solutions do not contain debris. Again, this is probably due to the lowered repulsive force between the particles due to the high ion concentration. The raft does not fall apart as it transforms to hematite. Thus, it transfers the angular morphology as a template. Further evidence that the cube shape has been templated is that this morphology is not the equilibrium shape of the particles. If a solution of cubes is aged, the particles become more rounded. This is evident not only from this work, but also from the work of DeBlanco *et al.* (15).

SUMMARY

The results of this study indicate that the size and aggregation of the metastable phase influences the morphology of the final particle. This study provides no support for a mechanism of simultaneous nucleation and aggregation for particles formed by the forced hydrolysis of ferric chloride solutions. Instead, direct evidence is seen for heterogeneous nucleation of hematite on akaganéite for the double-ellipsoid

and cube-shaped particles, and indirect evidence is obtained for the sphere-shaped particles. This heterogeneous nucleation allows the rods to act as templates which determine the morphology of the hematite particles. The starting concentrations of the reagents control the size of the akaganéite rods via the degree of supersaturation which determines the nucleation rate and amount of material precipitated. The starting concentrations also influence whether the akaganéite rods are aggregated or not. These colloidal interactions of the akaganéite rods are responsible for determining the shape of the template.

For the sphere-producing solution, the rods which form remain unaggregated in solution and the growth rate of the hematite is slow compared to the dissolution rate of the akaganéite so that the spheres do not have sufficient time to use the rod as a template before the rod dissolves. Spherical particles are formed in order to minimize surface energy. The spheres are not perfectly spherical, but are somewhat faceted. The double-ellipsoids nucleate on the unaggregated akaganéite rods which form, but in contrast to the spheres, the deposition of the iron from solution is faster than the dissolution of the rods, so in addition to growing outward from the rod, they begin growing along the length of the rods, forming a collar. Therefore the rods do act as a template for the double ellipsoids. The cubes are also formed from a template of the akaganéite, but for the cubes, the rods forming the template have aggregated into rafts. These rafts, which comprise rods of similar length, impart their cubical morphology to the hematite which nucleates on akaganéite in the raft.

This research provides insight into controlling the morphology of precipitated particles. Not only the kinetics, but also the colloidal interactions must be understood to control the formation of unusual particle morphologies. The concentrations of starting compounds influence both the kinetics of the reaction and the colloidal behavior. It is this influence on colloidal behavior that allows a similar chemistry, i.e., the chemistry of dissolution and redeposition of aqueous iron species, to produce radically different morphologies of precipitated particles.

ACKNOWLEDGMENTS

Portions of this work were completed by JKB and MLM at the University of Minnesota, Department of Chemical Engineering and Materials Science. The research at the University of Minnesota was funded by a grant from Sandia National Laboratories, Contract 05-3976. The cryo-TEM and portions of the dried sample TEM work were completed with the facilities of the Center for Interfacial Engineering at the University of Minnesota. The remaining TEM work was completed at the Electron Microbeam Analysis Facility in the University of New Mexico, Department of Geology and Institute of Meteoritics.

REFERENCES

1. Matijevic, E., and Scheiner, P., *J. Colloid Interface Sci.* **63,** 509 (1978).
2. Kerker, M., Scheiner, P., Cooke, D. D., and Kratohvil, J. P., *J. Colloid Interface Sci.* **71,** 176 (1979).
3. Hsu, W. P., and Matijevic, E., *Appl. Opt.* **24,** 1623 (1985).
4. Ozaki, M., and Takamatsu, K., *Nippon Kagaku Kaishi* **12,** 1960 (1988).
5. Kallay, N., Barouch, E., and Matijevic, E., *Adv. Colloid Interface Sci.* **27,** 1 (1987).
6. Amal, R., Coury, J. R., Raper, J. A., Walsh, W. P., and White, T. D., *Colloids Surf.* **46,** 1 (1990).
7. Paterson, R., and Smith, A. M., *J. Colloid Interface Sci.* **124,** 581 (1988).
8. Tang, H.-X., and Strumm, W., *Water Res.* **21,** 123 (1987).
9. Blesa, M. A., and Matijevic, E., *Adv. Colloid Interface Sci.* **29,** 173 (1989).
10. Baes, C. F., and Mesmer, R. E., "The Hydrolysis of Cations," p. 229. Wiley, New York, 1976.
11. Paterson, R., and Rahman, H., *J. Colloid Interface Sci.* **94,** 60 (1983).
12. MacKay, A. L., *Mineral. Mag.* **32,** 545 (1960).
13. MacKay, A. L., *Mineral. Mag.* **33,** 270 (1962).
14. Flynn, C. M., Jr., *Chem. Rev.* **84,** 31 (1984).
15. DeBlanco, E. K., Blesa, M. A., and Liberman, S. J., *React. Solids* **1,** 189 (1986).
16. Murphy, P. J., Posner, A. M., and Quirk, J. P., *J. Colloid Interface Sci.* **56,** 284 (1976).
17. Murphy, P. J., Posner, A. M., and Quirk, J. P., *J. Colloid Interface Sci.* **56,** 312 (1976).
18. Atkinson, R. J., Posner, A. M., and Quirk, J. P., *Clays Clay Miner.* **25,** 49 (1977).
19. Bailey, J. K., Nagase, T., Broberg, S. M., and Mecartney, M. L., *J. Non-Cryst. Solids* **109,** 198 (1989).
20. Bailey, J. K., and Mecartney, M. L., *Colloids Surf.* **63,** 151 (1992).
21. Bailey, J. K., Nagase, T., Pozarnsky, G. A., and Mecartney, M. L., *in* "Better Ceramics through Chemistry IV" (B. J. J. Zelinkski, C. J. Brinker, D. E. Clark, and D. R. Ulrich, Eds.), Mater. Res. Soc. Symp. Proc., Vol. 180, p. 759, Materials Research Society, Pittsburgh, 1990.
22. Bailey, J. K., Bellare, J. R., and Mecartney, M. L., *in* "Sample Preparation for Transmission Electron Microscopy" (J. C. Bravman, R. M. Anderson, and M. L. McDonald, Eds.), Mater. Res. Soc. Symp. Proc., Vol. 115, p. 69. Materials Research Society, Pittsburgh, 1988.
23. Bellare, J. R., Davis, H. T., Scriven, L. E., and Talmon, Y., *J. Electron Microsc. Tech.* **10,** 87 (1988).
24. Matijevic, E., *Acc. Chem. Res.* **14,** 22 (1981).
25. Brinker, C. J., and Scherer, G. W., "Sol–Gel Science," p. 237. Academic Press, New York, 1990.
26. Hiemenz, P. C., "Principles of Colloid and Surface Chemistry," p. 677. Dekker, New York, 1986.
27. Heller, W., *in* "Polymer Colloids II" (R. M. Fitch, Ed.), p. 153. Plenum, New York, 1980.